Applied Materials Today 28 (2022) 101507

Contents lists available at ScienceDirect

Applied Materials Today

journal homepage: www.elsevier.com/locate/apmt

Natural based reusable materials for microfluidic substrates: The silk road towards sustainable portable analytical systems

Ricardo Brito-Pereira [a,b,c,d], André S. Macedo [c,d,e], Clarisse Ribeiro [c,d,f], Vanessa F. Cardoso [a,b,c,d,*], Senentxu Lanceros-Méndez [c,d,g,h,*]

[a] CMEMS-UMinho, University of Minho, 4800-058, Guimarães, Portugal
[b] LABBELS-Associate Laboratory, Braga/Guimarães, Portugal
[c] CF-UM-UP, Centro de Física das Universidades do Minho e Porto, Universidade do Minho, Campus de Gualtar, 4710-057 Braga, Portugal
[d] LaPMET - Laboratory of Physics for Materials and Emergent Technologies, Universidade do Minho, 4710-057, Portugal
[e] IB-S, Institute of Science and Innovation for Bio-Sustainability, Universidade do Minho, Campus de Gualtar, 4710-057 Braga, Portugal
[f] CEB, Centro de Engenharia Biológica, Universidade do Minho, Campus de Gualtar, 4710-057 Braga, Portugal
[g] BCMaterials, Basque Center for Materials, Applications and Nanostructures, UPV/EHU Science Park, 48940 Leioa, Spain
[h] IKERBASQUE, Basque Foundation for Science, 48009 Bilbao, Spain

ARTICLE INFO

Keywords:
Microfluidic
Point-of-care
Portable analytical devices
Silk
Sustainability

ABSTRACT

Portable analytical systems are versatile tools for application in areas including biomedicine, biosecurity, food safety and environmental monitoring. This work contributes to the increasing demand for low-cost, environmentally friendly substrates for portable analytical systems by using natural *Bombyx mori* cocoons. Further, silk fibroin is also extracted from these cocoons and electrospun into oriented and randomly oriented fiber substrates. Oxygen plasma treatment is applied to improve their hydrophilicity. Fiber morphology, mechanical properties, porosity, thermal characteristics and surface contact angle are extensively characterized and the ability of the samples for passive capillary flows demonstrated. Plasma treated pressed cocoons show superhydrophilicity, capillary flow rates of 44.8 ± 3.75 mm.min^{-1}, and high mechanical resistance with Young's modulus values up to 592.13 ± 19.83 MPa.

The developed materials are used as substrates for the colorimetric quantification of three commonly scrutinized clinical analytes. Hydrophobic barriers are first wax-printed on all samples with a proper design and albumin assays are performed on all substrates. Further assays for uric acid and glucose quantification are successfully accomplished on the pressed cocoons after a simple in between washing step, with overall high coefficient of determination, proving the suitability of the developed materials as low-cost, sustainable and reusable microfluidic substrates.

1. Introduction

Prevalence of diseases often associated with bad nutritional habits or poor lifestyles in regions that suffer from inequality of income and a lack of access to medical supervision has been rising. In Germany, by 2040, an increase ranging from 54% to 77% of the incidence of type 2 diabetes has been projected [1]. High serum uric acid levels have been linked to prediabetes [2], as well as an increased risk of cardiovascular diseases [3], gout and renal calculi [4]. Low blood albumin levels can be caused by liver diseases such as cirrhosis or hepatitis [5], infections, general inflammation, as well as malnutrition and malabsorption [6]. The populace of third-world countries, where resources are scarcer, especially struggle with the latter. These data demonstrates there is a strong need for inexpensive, easy to use, fast and sustainable portable analytical devices capable of not only early medical diagnosis and low-cost periodic monitoring of specific health conditions, but also for other applications such as detection of water contaminants [7] or food safety [8].

Portable analytical systems, which encompass point-of-care (POC) systems in the biomedical field, are diagnostic tools suitable to assist in solving of those issues, allowing *in situ* preliminary evaluation that can be followed up accordingly [9]. Microfluidic paper-based analytical devices (μPADs), first introduced by Martinez et al. [10], who created hydrophobic channel walls using photolithography on *Whatman*® filter

* Corresponding author.
E-mail addresses: vcardoso@cmems.uminho.pt (V.F. Cardoso), senentxu.lanceros@bcmaterials.net (S. Lanceros-Méndez).

https://doi.org/10.1016/j.apmt.2022.101507
Received 8 February 2022; Received in revised form 28 March 2022; Accepted 1 May 2022
Available online 13 May 2022

paper, are one type of portable analytical systems particularly appealing due to their portability, versatility, ease of use and low-cost [11–13]. Hydrophobic channels for the development of portable analytical devices have been also implemented by plotting [14], inkjet [15], screen [16] or wax printing [17]. The latter has been used, among others [18], to develop portable analytical systems able to carry out colorimetric assays, where a reaction between one or more reagents and an analyte generates a color change that may correspond to either the simple presence or a more exact quantification of the specific analyte [19]. The most common paper-based substrates are composed of filter paper, chromatography paper, nitrocellulose membrane, and paper/polymer or paper/nanomaterial composites [20]. Other substrates such as cotton thread have been evaluated as substrates for discriminating DNA mismatches that lead to genetic diseases [21]. Research is being developed to complement the commercially available paper-based substrates, by exploring alternative synthetic polymer-based microfluidic substrates such as poly(L-lactic acid) (PLLA) [22] or poly(vinylidene-*co*-trifluoroethylene) (PVDF-TrFE) [23], which have higher mechanical strength and tunable morphology and porosity. However, more sustainable materials and processing methods must be achieved in order to avoid the chemical processing need to produce the aforementioned microfluidic substrates, which in the case of cellulose usually also requires complex processes including wood preparation, pulping, chemical recovery, bleaching, and papermaking to convert wood to the final product [24, 25].

In fact, in the present day, together with improving the performance of devices, one of the most urgent needs is increasing sustainability of materials and processes, in particular in the area of disposable devices [26]. In fact, the amount of waste produced per hospital patient per year varies greatly worldwide, from 0.44 kg in Mauritius to 8.4 kg in the United States of America (USA) [27], here with an additional 50.000 tons generated from home healthcare annually [28]. This waste is a danger to global health and the environment, and thus the search for natural, reusable, and renewable materials, as well as the use of sustainable processing techniques and general circular economy concerns has been met with investment [29]. The development of reusable portable analytical diagnostic devices based on sustainable materials represent one way to address this problem.

Silk fibroin (SF), a biocompatible and biodegradable fibrous protein [30] with mechanical strength and thermal resistance [31], can be extracted from a number of arthropods including spiders and silkworms [32], most typically from *Bombyx mori* (*B. mori*) cocoons, as is the case of the present work. The silk filament is composed of sericin (the outer coating) and fibroin (the inner brins) [33]. SF can be processed into a variety of formats and has been extensively used in applications as diverse as scaffolds [34] for tissue engineering and *in vitro* disease models or drug delivery in the form of hydrogels, microspheres or films [35,36], combined with polyethylene oxide to create air filtration systems [37], as substrates for wearable displays [38], and often together with graphene in electronic applications such as bio-integrated electrode systems [39], pressure sensors [40], or enzymatic biosensor transistors [41]. As an example, graphene nanosensors printed on water-soluble silk films have been developed for bioselective bacteria detection on tooth enamel [42]. A flexible, fully organic, biodegradable and label-free impedimetric biosensor has been also reported, for the detection of vascular endothelial growth factor (VEGF). The biosensor has been fabricated by photolithography and using flexible fibroin as substrates [43]. Silk yarn coated with conducting inks and appropriate reagents have been woven into glucose sensors as a cost-effective solution and using lower solvent quantities than traditional screen-printing [44]. Although some studies have evaluated the general properties of whole silk cocoons [45], mainly addressing their permeability [46] and electrical properties [47], their use as microfluidic substrates seems to be somewhat rare, although they have been employed, for example, to develop immunosensing assays for red blood cell antigen typing [48].

Regarding processing techniques, electrospinning is a technique that allows the development of fiber matts by applying a high voltage electrical field to a droplet of polymeric solution, typically fed through a syringe with a metallic needle by a pump, giving rise to a jet that is collected in a metallic platform. The intensity of the electrical field, solution concentration, pumping rate and distance to the collector regulate fiber shape and size. Oriented fibers can be obtained by using a rotating collector [49]. Electrospun (ES) SF mats have been prepared by tailoring diameter and thickness for controlled drug release [50], modified with graphene oxide to improve antibacterial activity and biocompatibility [51], or carbon nanotube composites for enhancing cardiomyocyte functionalities [52].

Further, the surface characteristics and wettability of SF fiber mat can be modified by plasma treatment, where functional groups are introduced to the surface of the exposed material changing its composition, improving the bonding of water molecules by integrating C=O bonds [53,54].

Herein we report on pressed silk cocoons and ES SF substrates for the development of natural-based reusable portable analytical systems. Together with their processing and characterization, their suitability to carry out colorimetric quantification of clinically relevant analytes is demonstrated.

2. Experimental methods

2.1. Materials

B. mori silkworm cocoons were supplied by *APPACDM* from Castelo Branco (Portugal). Sodium carbonate (Na_2CO_3), formic acid (FA, CH_2O_2), calcium chloride ($CaCl_2$), absolute ethanol (C_2H_5OH) and Hach pH 4.01 buffer solution were obtained from *Sigma-Aldrich*. Distilled water was prepared in the laboratory. All reagents and solvents were used as received.

2.2. Bombyx mori silkworm cocoons-based substrates processing

The cocoons were first cleaned by scraping major impurities from its inside, and cut in 30 mm^2 pieces and then subjected to a mechanical press (*Model 4350.L Bench Top, Carver, Inc.*, USA) at a pressure of 5 tons for 3 h, reducing their thickness and making them flat and suitable for printing. Raw cocoons and pressed cocoons will be addressed as R-cocoons and P-cocoons, respectively.

2.3. Randomly oriented and oriented electrospun fiber substrates processing

The extraction of SF from *B. mori* silkworm cocoons was carried out by a soap degumming method. Cocoons were cleaned, cut in 1 cm^2 pieces and boiled in a 0.05 wt% Na_2CO_3 solution for 30 min in a silk to water solution ratio (w/v) of 1:40. The resultant fibers of SF were thoroughly washed with distilled water and dried at room temperature for 24 h. These fibers were then dissolved in a 0.17 M solution of FA/$CaCl_2$ with a ratio of 12:1 v/w (FA:SF). To remove impurities, this solution was centrifuged (*Hettich EBA 21*) at 6000 rpm for 10 min and the supernatant SF/FA/$CaCl_2$ solution was cast on a petri dish and left to dry at room temperature for 24 h to allow the FA to evaporate. The resultant transparent and plastic material was once again washed in a distilled water bath to remove $CaCl_2$ and dried at room temperature for 24 h, leading to brittle, whitish solid SF. Then, SF was dissolved in FA (8:1 v/w FA:SF) during 1 h to obtain a solution suitable for electrospinning. The SF/FA solution was transferred to a 10 mL disposable syringe fitted with a blunt steel needle, with an inner diameter of 0.41 mm, and placed in a syringe pump (*New Era NE-1000*). Electrospinning was conducted using a high voltage power supply (*Glassman PS/FC30P04*) set at 20 kV and the solution was pumped at a flow rate of 0.5 $mL.h^{-1}$. The resulting randomly oriented ES SF samples were collected on a grounded 20 × 15 cm static plate collector placed 15 cm away from the tip of the needle.

Oriented ES SF samples were obtained using the same process as the one described before except for the use of a grounded rotating drum collector set at a speed of 1500 rpm. ES samples will be referred as O-ES and RO-ES for oriented and randomly oriented SF membranes, respectively.

2.4. Surface modification by plasma treatment

P-cocoons, O-ES and RO-ES samples were subjected to plasma treatment in order to obtain superhydrophilic substrates [55]. The surface treatments were conducted in a plasma chamber (*Diener Electronics Zepto*) equipped with a 40 kHz radio frequency plasma generator using oxygen (O_2). Base pressure before plasma irradiation was 20 Pa. 50 W of power were applied for 100 s under a total pressure of 80 Pa. This procedure was performed on both surfaces of the samples. Samples without and with O_2 plasma treatment will be identified as w/o and w/ plasma, respectively.

2.5. Sample characterization

2.5.1. Physicochemical characterization

A scanning electron microscope (*FEI Nova 200*) was employed for the characterization of the morphology and fiber size of all samples, which were previously sputtered with a thin gold layer (*Polaron SC502*). Mean fiber diameter was calculated from measuring approximately 50 fibers using the *ImageJ* software.

The porosity of the samples was measured by liquid displacement using a pycnometer. The weight of the pycnometer filled with ethanol was measured and labelled as W_1 . The samples, whose weight was W_S, were immersed in ethanol. After the sample was saturated, additional ethanol was added to completely fill the volume of the pycnometer, and the device was weighed (W_2). The sample was then taken out of the pycnometer and the weight of the system with ethanol was labelled W_3 . The porosity of the sample was obtained as the average of three values according to $\varepsilon = (W_2 - W_3 - W_S)/(W_1 - W_3)$. Absolute ethanol, as a non-solvent for all samples, was used as displacement liquid since it can penetrate the pores without inducing either shrinking or swelling. The assays were performed on hydrophobic samples before plasma treatment, since plasma treated samples absorb the ethanol into the matrix which would lead to porosity measurement errors.

Mechanical properties were evaluated in the tensile mode with a *Shimadzu AD-IS* universal testing set up using a load cell of 50 N for ES samples and 500 N for P-cocoons samples. 15 mm long and 10 mm wide samples were stretched at a rate of 1 mm.min^{-1}. O-ES samples were stretched along the direction of the fibers. Sample thickness averaged 110, 103 and 81 μm for P-cocoons, RO-ES and O-ES samples, respectively, as measured using a *Fischer Dualscope MPOR*. The stress-strain measurements were performed in triplicate on dry and wet samples, using 40 μL of water in the latter.

FTIR-ATR were performed at room temperature in all samples with a *Bruker Alpha II*, from 1000 to 2000 cm^{-1} using 64 scans and a resolution of 4 cm^{-1}. The degree of crystallinity of the P-cocoons, O-ES and RO-ES samples w/o and w/ plasma treatment was calculated according to $X_C = (A_{1263}/(A_{1230} + A_{1263})) \times 100$, comparing the absorption bands intensity ratio at approximately 1263 cm^{-1} and 1230 cm^{-1} assigned to amide III associated to β-pleated-sheet conformation and random-coil conformation, respectively, from the FTIR-ATR spectra [56].

Thermal characteristics of the samples was evaluated by DSC in a *PerkinElmer 6000*. Samples weighing approximately 6 mg were placed into 40 μL aluminum pans and then heated from 30 to 400 °C at a rate of 10 °C.min^{-1} after an initial heating (and cooling back) from 30 to 100 °C at a rate of 20 °C.min^{-1}. This first cycle was carried to promote the evaporation of the solvent and the water molecules that could be included in the polymer structure.

2.5.2. Contact angle and capillary flow rate assays

Surface wettability was evaluated using the sessile drop method with a *Data-Physics OCA20*, by measuring the CA of 3 μL ultrapure water drops on all samples. Six measurements were carried out for each sample in different zones of the samples to obtain the mean CA and standard deviation.

2.5.3. Colorimetric quantification of albumin, uric acid and glucose

The preparation of the portable analytical systems is illustrated in Fig. 1. The design was created using computer-aided design software (*Sketchup* 2017) and printed with a *Xerox ColorQube 8880* printer. After printing, each substrate (including P-cocoons, RO-ES and O-ES) were placed on a hot plate (*Prazitherm P272*) at 100 °C for 2 min for the wax to penetrate the samples all the way through to the opposing surface, so the barriers can fully contain the fluids. Each system comprises three reaction chambers that act as replicas, an inlet, and a control chamber. The diameters of the reaction and control chambers are 4 mm, the diameter of the inlet is 4.5 mm and the channels connecting the inlet to the reaction chambers are 9 mm long and 2 mm wide. These dimensions shrunk around 15% during the curing process due to wax expansion. A total of four systems corresponding to four different measurement concentrations were printed for each type of substrate.

Colorimetric quantification assays for albumin, uric acid and glucose were performed using commercial kits (*Trinder – Endpoint, FAR Diagnostic*). In all cases, the reaction chambers were first functionalized using 15 μL of the analyte solution under study (albumin, uric acid or glucose) and left to dry for approximately 5 min. For the albumin assay, as correct color complex formation depends on the acidity/basicity, a buffer solution of pH 4.01 was previously added to uniform the pH of the different substrates. Then, the reagent was pipetted into the inlet of the microfluidic system, reaching the reaction chambers by capillarity. After an appropriate time with depends on the analyte being used, the corresponding color variation occurred. The substrates were then scanned (*Brother DCP*-1610 W) and color analysis was performed with *ImageJ* software by measuring the mean gray values of each reaction chamber. These results were used to obtain the calibration curves.

As firt approach, albumin quantification was performed on all types of substrates. In this specific case, albumin reacts with bromocresol green at a pH of 4.01 inducing a change to green color. Calibration curves were determined using albumin concentrations of 100, 200, 1000, and 4000 mg.dL^{-1}.

As the plasma treated P-cocoons were perfectly viable for carrying the colorimetric tests, their natural quality (only pressed, without the need of any chemical processing) makes them extremely interesting candidates for reusable and thus sustainable microfludic substrates. As such, only P-cocoons were used for the consecutive quantification of albumin, followed by uric acid and then glucose, by means of a washing step in between uses. The substrates were placed under subtle agitation at a temperature of 60 °C, in a solution with a small amount of dissolved biodegradable pink soap, rinsed in water, and left to dry before carrying out another assay. Uric acid is transformed into allantoin in the presence of uricase, with formation of hydrogen peroxide which, in presence of peroxidase, reacts with ethyl-sulphopropyl-toluidine and 4-aminophenazone to produce a violet/purple complex whose color intensity is directly proportional to the concentration of uric acid in the samples. Concentrations of 0.5, 1, 2 and 5 mg.dL^{-1} were used. The substrates were once again washed, and the glucose assay was carried out. Glucose is oxidized into gluconic acid and hydrogen peroxide by glucose oxidase. Hydrogen peroxide reacts with phenole and 4-aminophenazone in the presence of peroxidase, producing a red/orange complex whose color intensity is directly proportional to the glucose concentration in the samples. These tests were carried at concentrations of 50, 100, 150 and 200 mg.mL^{-1}. Reaction time for glucose and uric acid is around 10 min, while for albumin is below 1 min.

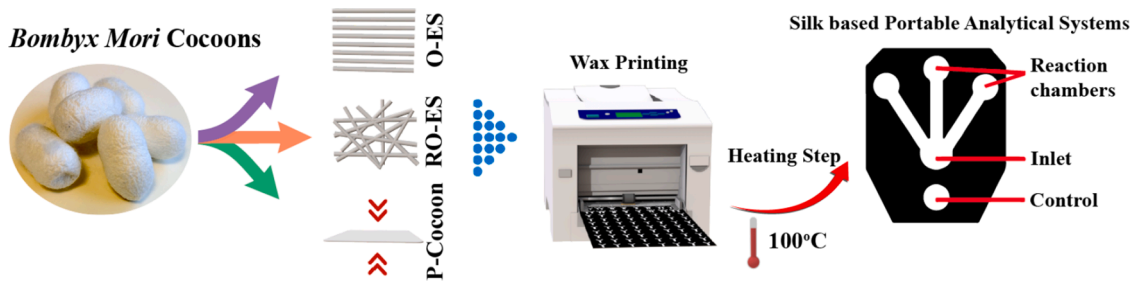

Fig. 1. Procedure for fabrication of the silk-based portable analytical system involving wax printing.

3. Experimental results and discussion

3.1. Physicochemical characterization

Representative Scanning Electron Microscopy(SEM) images of the P-cocoons, O-ES and RO-ES samples, w/o and w/ plasma treatment, are shown in Fig. 2a. R-cocoons were also analyzed to evaluate any change of their micromorphology that could arise from the pressing process. Fiber diameter, represented in Fig. 2b, influences the structural and physical properties of the samples, including porosity (Fig. 2c), mechanical strength and capillary flow rate [40].

ES samples present cylindrical oriented and randomly oriented fibers according to the processing conditions. The *B. mori* cocoons exhibit a relatively smooth surface even before pressing (R-cocoons), but more so when pressed (P-cocoons). After plasma treatment, there appears to be no evidence of removal of the silk sericin layer in the P-cocoons samples. Overall, the characteristic fiber distribution and multilayered structure, as well as their interconnectivity, and diameter were reasonably preserved in all samples, independently of the processing conditions. Very slight differences in terms of fiber surface texture can be observed when comparing pre and post plasma treatment, as has been previously reported [54]. This confirms that the O_2 plasma treatment did not significantly modify the morphology of the samples at the microscale, as the treatment protocol was previously optimized [57] not only to minimize overheating or significant morphological changes, but also to ensure the stability of the hydrophilic surface over time, as the samples were tested and remained hydrophilic after 3 months.

RO-ES samples, w/o and w/ plasma treatment, are characterized by mean fiber diameters of 914 ± 21 nm and 806 ± 14 nm, respectively, while O-ES samples present slightly lower diameters of 787 ± 19 nm and

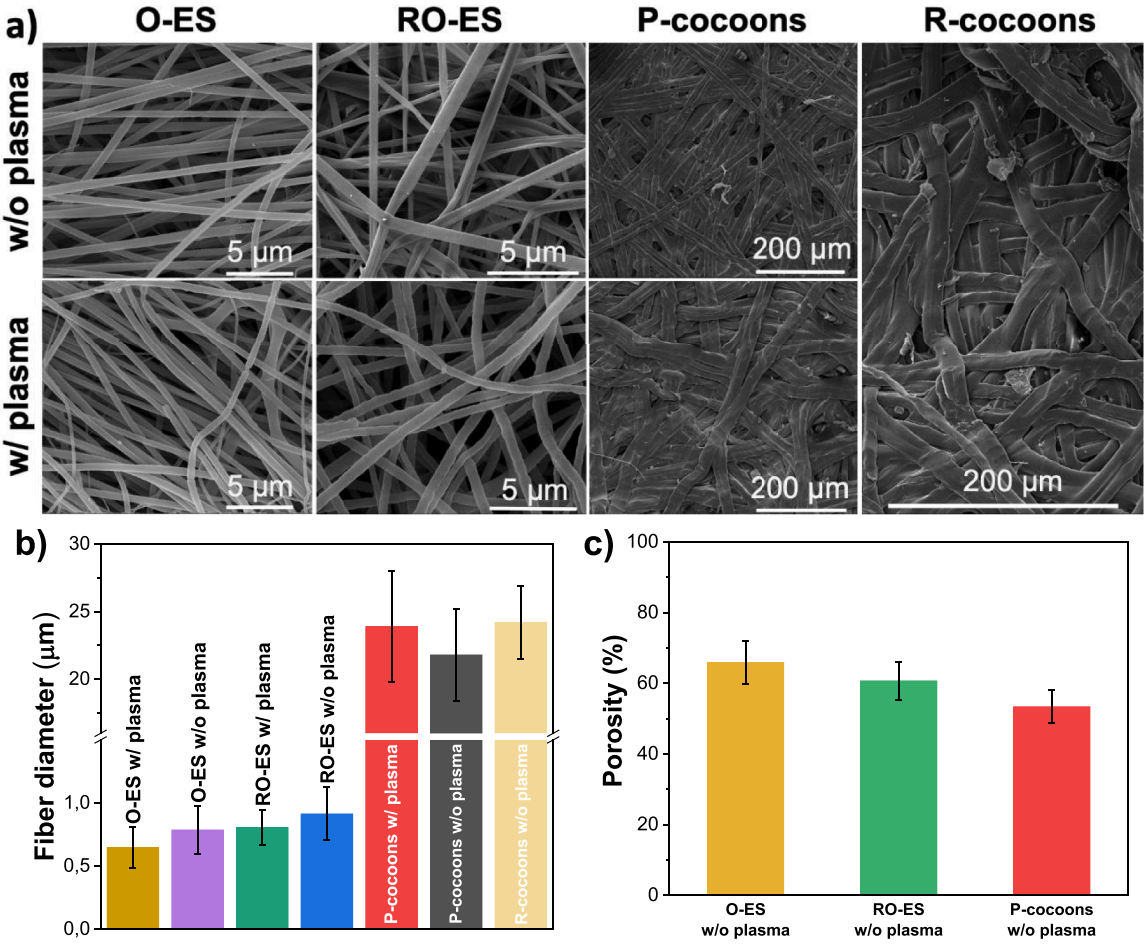

Fig. 2. a) Representative SEM images of processed samples w/o and w/ plasma treatment. Image of R-cocoons is also presented, and b) Respective fiber diameters; c) Porosity of the samples w/o oxygen plasma treatment.

648 ± 20 nm, respectively. The smaller size of the oriented fibers results from stretching during their collection in the rotating drum [58]. A slight decrease in average fiber diameter after plasma exposure is observed and also in agreement with the literature [59]. This can be attributed to the applied atmosphere pressure and heating during the treatment which promotes evaporation of the solvent remnants. *B. mori* cocoons' average fiber widths are significantly larger than for ES SF samples, both as R-cocoons and P-cocoons. These sizes are at the micrometer scale, with values of 24.2 ± 2.7 μm for R-cocoons and 21.8 ± 3.4 μm and 23.9 ± 4.1 μm for P-cocoons, w/o and w/ plasma treatment, respectively. The slight increase of the average fiber size after plasma treatment may be attributed to the local heating of sericin and leading to fiber dilatation by releasing the effect of the applied pressure. Further, differences can also be expected due to the natural variations between samples produced by *B. mori* [60]. Another important observation is that the *B. mori* cocoons' morphology and average fiber widths are very similar to the commonly used *Whatman* n°1 cellulose filter paper [22] (the gold standard on POC applications after its introduction [10]). However, although both materials come from natural sources, P-cocoons, which are white by nature, require no further processing beyond pressing and plasma treatment, contrary to cellulose that typically requires complexes processes, including wood preparation, pulping, chemical recovery, bleaching, and papermaking to convert wood to the final product [24][26].

Another important parameter is porosity, which is one of the main factors that affects how solutions behave when interacting with a sample, which is essential to evaluate for printable materials and their applications in portable analytical systems. Nonetheless, the assays were performed on hydrophobic samples before plasma treatment, since plasma treated samples absorb the ethanol into the matrix which would lead to porosity measurement errors (as explained in Section 2.5.1). Porosimetry results (Fig. 2b) show that O-ES samples are characterized by a porosity of 65.9 ± 6.1%, followed by the RO-ES samples with 60.7 ± 5.45%. As the fibers in these samples are similar in size, the more the fibers are randomly deposited one above the other, the tighter the spaces between them, explaining the lower value in the RO-ES samples. Cocoons, with similar non-oriented fiber morphology, present a degree of porosity of 53.4 ± 4.7%. *B. mori* fibers are flatter than the cylindrical electrospun fibers, which promotes a lower porosity due to their ability to be deposited in a more compact way.

Stress-strain mechanical curves and the corresponding Young's modulus, Fourier-transformed infrared spectroscopy measurements in attenuated total reflectance mode (FTIR-ATR) spectra, and differential scanning calorimetry (DSC) thermograms for the different samples are presented in Fig. 3.

Mechanical stability of microfluidic substrates used for the development of portable analytical systems is essential, as samples must be able to withstand wear and tear that may come from simple user manipulation or repeated washing and reutilization.

Stress-strain curves up to 15% (Fig. 3a) reveal highly deformable structures at low forces, with the mechanical characteristics being determined by a deformation of the network structure and not of the material itself [61]. P-cocoons possess a much higher resistance to deformation when compared with the ES samples, due to their larger fiber diameter. The ES samples reveal an earlier plastic regime, with the O-ES samples possessing higher resistance than RO-ES, as the aligned fibers allow the sample to withstand higher forces [23]. O-ES samples in dry state reach Young's modulus values of 348.23 ± 16.16 MPa (276.96 ± 12.09 MPa when wet), close to, but still inferior to the wet P-cocoons (377.2 ± 13.39 MPa, Fig. 3b). The lowest values correspond to the

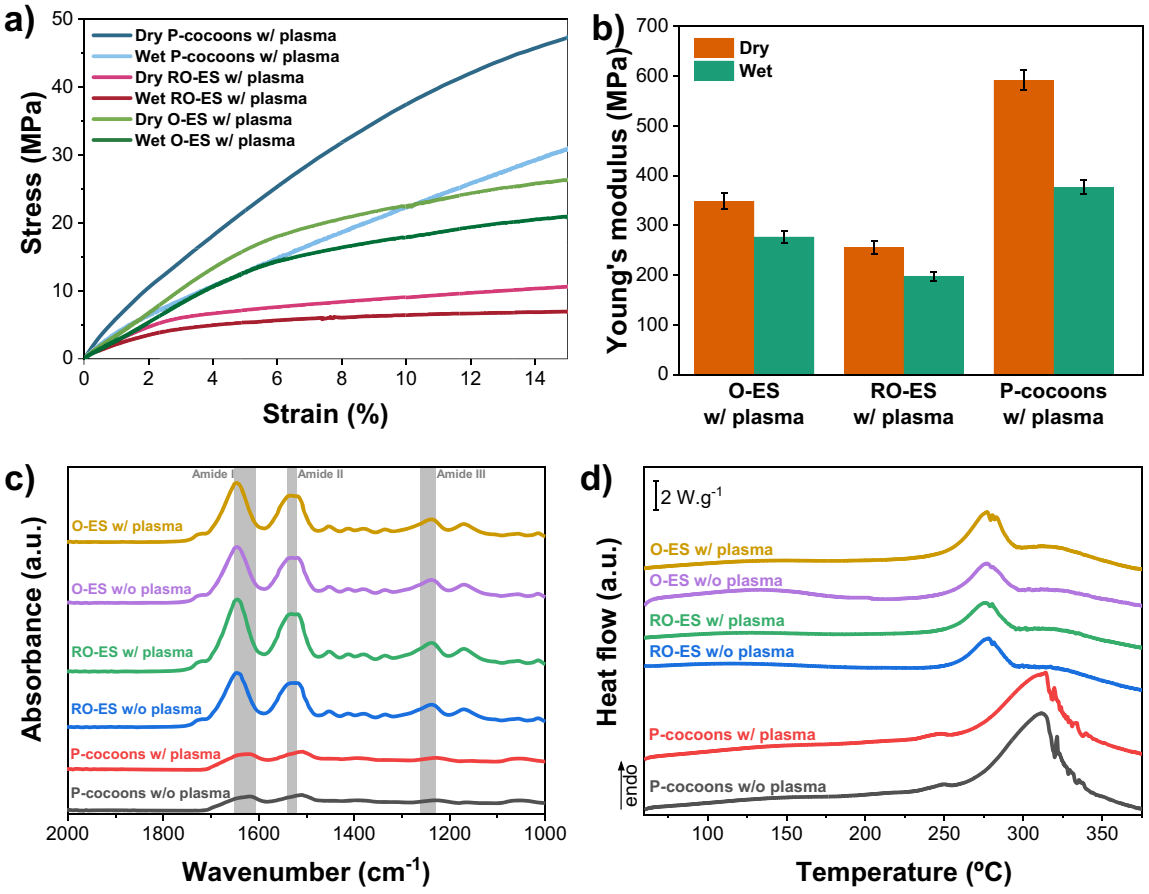

Fig. 3. a) Stress-strain curves up to 15% of strain, and b) Respective elastic modulus for the plasma treated samples in dry and wet states; c) FTIR-ATR spectra and d) DSC thermograms of the processed samples.

RO-ES fibers (255.54 ± 13.46 MPa and 198.18 ± 9.04 MPa in the dry and wet states, respectively), concurrently revealing they possess the lowest linear regime capacity, quickly giving way to plastic regime. The fact that the stress-strain measurements were taken in the direction the fibers were spun (not perpendicularly) explain the higher resistance of O-ES samples when compared to the RO-ES samples [61]. The P-cocoons' superior strength can be attributed to greater fiber-size, as well as the presence of sericin which has been shown to enhance the tensile properties of regenerated silk filament [62]. As is later proven by the proofs of concept, these values show the samples are more than able to withstand the conditions necessary for carrying aqueous assays. Moreover, all samples are consistently more resistant to mechanical deformation when dry. P-cocoons present the highest elastic modulus, with values of 592.13 ± 19.83 MPa in a dry state and 377.2 ± 14.39 MPa when wetted.

FTIR spectra (Fig. 3c) of samples w/o and w/ plasma treatment show no relevant differences among them, indicating that the use of O_2 plasma does not induce any significant chemical change. Amide I (which corresponds to C=O stretching) and II (N—H in-plane bending) bands with peaks at 1616 and 1508 cm^{-1} are evident in the P-cocoons' spectra, with a clear shift to higher wavenumbers for all RO-ES and O-ES samples, peaking at 1648 and 1527 cm^{-1} respectively. The bands corresponding to Amide III (–N and N–H functionalities) at around 1263 and 1230 cm^{-1} are less apparent but may also be correlated with an alteration of the secondary structure, an increase of the relative proportion between the random coils and β-sheet conformations [60,63]. This alteration can be attributed to the slow solvent evaporation during the electrospinning process, which leads to improved polymer chain organization and consequentially a highly crystallized structure [64]. The lower peaks in the P-cocoons samples for Amide I, II and III may be due the presence of sericin which seems to have an effect of masking the fibroin and of attenuating the vibrational peaks, as sericin is present as a sheath over the fibroin core of the fiber [65].

The degree of crystallinity of the different samples was calculated from the FTIR-ATR spectra, and the results are shown in Table 1.

Mean crystallinity degrees of approximately 47% and 43% were obtained for the P-cocoons and ES SF samples, respectively. This difference is within experimental margin considering the natural origin of the cocoons and the typical variations between samples [66], which can slight change the physical properties of *B. mori*. No variations in the degree of crystallinity of the samples are observed due to the plasma treatment, as its effect is restricted to the fiber surface [57].

Fig. 3d shows the DSC thermograms of the different samples for a heating scan from 60 to 375 °C. P-cocoons show the endothermic peak at 310 °C associated with the heat-protective sericin layer [67]. Silk I conformation, an organized, crystalline form of fibroin, transforms into the β-sheet structure of silk II with the application of mechanical strain or other energy inputs. The presence of silk II or both I and II is correlated with the endothermic peaks at higher temperatures [68], and a larger presence of silk II crystalline domain may have been induced by the pressing of the cocoons. O-ES and RO-ES samples show the characteristic endothermic peak around 280 °C due to the degradation of highly crystalline SF structures, specifically the side chains groups amino acid residues and the cleavage of peptide bonds [64,69]. This lower temperature peak is ascribed to the sole presence of fibroin in the ES samples, as opposed to fibroin and sericin in the P-cocoons. There are no significant changes between the samples w/o and w/ plasma, as the treatment only acts at the surface level.

Table 1
Crystallinity degree of the P-cocoons and ES SF samples.

Sample	X_C (%)
P-cocoons w/o plasma	47.6 ± 1.9
P-cocoons w/ plasma	47.3 ± 1.9
RO-ES w/o plasma	43.2 ± 1.7
RO-ES w/ plasma	42.9 ± 1.7
O-ES w/o plasma	43.1 ± 1.7
O-ES w/ plasma	42.9 ± 1.7

3.2. Contact angle and capillary flow rate assays

Contact angle (CA) and capillary flow rate results are presented in Fig. 4.

The hydrophobic nature of *B. mori* and ES samples is a key issue that must be overcome for their use as microfluidic substrates, where capillary flow is essential. Surface wettability is governed by surface chemistry, surface energy and morphology as well as by the properties of the solution [70]. CA is the most used method to measure these properties and provides accurate results about the wettability of materials and was used in both P-cocoons and ES SF samples [54,60].

Morphology and plasma treatment have a direct effect on water CA values and therefore on surface wettability (Fig. 4a). Untreated P-cocoons samples have a mean CA value of 130 ± 4.5 °, representing a slightly hydrophobic behavior when compared to the ES samples which have lower CA values of 117.7 ± 3.4° and 104.1 ± 3.8° for the RO-ES and O-ES samples, respectively. This difference can be explained by the higher surface roughness of the P-cocoons samples when compared to the ES samples, as well as differences in terms of compactness, crystallinity, and composition as cocoons still possess sericin, while the ES samples are only composed of fibroin [71]. The CA of all plasma treated samples decreased to 0°, with the water drop being completely absorbed in less than 30 s, when brought in contact with the surface. The reduction of the CA value is a clear indication of the increase in wettability, demonstrating a superhydrophilic behavior, based on the introduction of C—O and C = O groups, being stable for at least 3 months, as previously indicated [57].

Capillary flow rate evaluation ascertains the ability of the samples to generate passive capillary flow, without the need for external actuation systems. The results for the different samples can be found in Fig. 4b. The samples w/o plasma treatment show no visible capillary flow, as expected due to their hydrophobic nature. P-cocoons and RO-ES samples w/ plasma treatment are characterized by similar flow rates: 44.8 ± 3.75 and 46.5 ± 2.05 $mm.min^{-1}$, respectively. The closeness of these results is related to the similar microstructural features governed by the non-oriented fibers, with the differences in fiber diameter seemingly having no effect on capillary flow. Oriented fibers allow solutions to follow a specific direction without obstruction from transversal fibers, as is verified by the higher mean value of capillary flow, 82.1 ± 4.95 $mm.min^{-1}$. This tunable capillary flow rates according to the sample morphology is a valued property that can be taken into account, depending on the application requirements.

3.3. Albumin, uric acid and glucose colorimetric assays on silk substrates

After wax-printing the pattern for the portable analytical system (described in Section 3), colorimetric analysis for albumin was first carried out for all the silk-based substrates under study subject to plasma treatment. These tests are depicted in Fig. 5a.

Overall, print quality and wax adhesion varies for each substrate. The ES SF substrates show more defined borders in comparison to the P-cocoons substrates, all of them w/ plasma, as expected given the cocoons' more irregular surface even after pressed. On the other hand, wax adhesion is improved in the P-cocoons. Electrospinning produces thinner fibers than those of natural P-cocoons, which are also deposited in a much more compact manner, leading to smaller interstices. This may explain the absence of wax at certain spots in the ES substrates, which nevertheless did not hinder the applicability of the materials. The same principle applies to the P-cocoons: as the interstitial spaces between fibers are wider, vestigial spaces that were not filled with wax during the thermal curing process may allow small leakages of fluid beyond the printed frontiers, as is observed in Fig. 5a. This did not affect

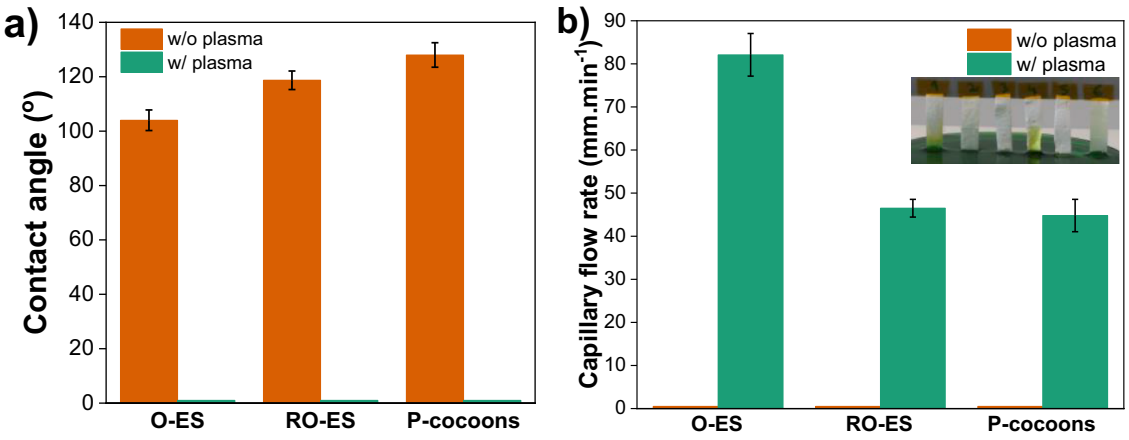

Fig. 4. a) Contact angle and b) Capillary flow rates in the antigravity direction of a dye solution for the processed samples.

the assays in any of the cases, immediately apparent by the color formation which gradually grows in intensity as concentrations increase, and also confirmed by mean gray value evaluation. The calibration curves for the albumin assay show that colorimetric assays on all substrates show linear fittings, with R^2 values of 0.992, 0.957 and 0.991 for RO-ES, O-ES, and P-cocoons respectively, demonstrating the strong correlation between variation in color intensity and concentration. The somewhat lower R^2 value for the O-ES substrate may be due to the more heterogeneous color formation within the reaction chamber due to fiber orientation. Nonetheless, with a value of 0.957, the correlation is still evident. The P-cocoons exhibit a lower slope value, which is associated with a lower sensitivity to the color gradient, which may be related with how the color tone is produced when contrasting with the substrate's own color. This is not detrimental for the assay, as the correlation is still very strong (R^2 of 0.991).

After the previous assays, P-cocoons samples were selected for their simple and sustainable processing to evaluate their possible reuse as microfluidic substrates. The samples were then cleaned according to the indicated protocol (described in Section 2.5.3) and uric acid colorimetric assays were performed, as illustrated in Fig. 5b. In addition to the reagent and sample used to carry the albumin colorimetric assay, the cleaning process removed some of the wax from the printed zone of the cocoons, as indicated by the lighter areas observed in some samples. In this sense, the cleaning process can be further optimized to better preserve the wax patterns. Nevertheless, the fluids are still mostly contained within the reaction chambers and color complex formation is clear, which is confirmed by the corresponding fitting. R^2 value decreased only slightly (from 0.991 to 0.983), showing that a strong correlation between concentration and color intensity is maintained. The slope value is closer to those observed in the ES substrates, higher than the albumin assay and hence an improvement towards the previous assay in the same P-cocoons. This may be due to a better contrast of the pigment when interacting with the substrate.

Substrates were once again cleaned and the glucose assays were carried, as shown in Fig. 5c. The cleaning process did not remove wax any further than in the previous assay, which suggests the amount of wax previously washed away was mostly excess from the surface. The leakage from the channels and chambers is slightly higher but the hydrophobic barriers still fulfill their role in containing the fluids. The R^2 value again decreases in a very small amount from 0.983 to 0.967, showing that a strong correlation is still present for the glucose assay. The slope value is considerably higher than the result from the uric acid assay (79.02 compared to 26.4), suggesting that the pigment may be even more adequate for this substrate. Reuse assays were also successfully performed on the ES SF substrates (data not shown).

3.4. Comparative evaluation with commercial paper-based substrates

The main properties featured by the developed plasma treated P-cocoons and ES SF membranes, together with the ones of two paper-based membranes commonly used as microfluidic substrates, are summarized in Table 2.

Although the papermaking process is mature, it involves complex procedures with high environmental impact and resources wear. In addition, their physicochemical properties are often not available, which means that the selection of the material(s) for the development of a specific portable analytical system is not always made according to the most appropriate properties to match the requirements of the proposed application (such as collection, separation, pre-concentration or mixing, among others), but rather according to the material available or the most cost effective. Thus, the present work proposes and duly characterizes an alternative material based on *Bombyx mori* cocoons, which is also of natural origin. Further, it is originally white, unlike paper that requires bleaching in addition to other chemical processes, which is a property required for colorimetric assays. The morphology of the substrates can be tailored by processing, allowing to tune capillary flow. O-ES SF membranes present the highest capillary flow due to fiber orientation, while the P-cocoons and the RO-ES SF membranes feature capillary flow rate similar to the commercial *Whatman™ no.1* membranes. Millipore HF090 membranes, in turn, present the lower capillary flow and require a backing transparent material. Moreover, all the prepared membranes are characterized by relatively good wax printing and colorimetric detection quality. However, P-cocoons stand out as they do not require any chemical process (just pressing and plasma treatment) and present excellent mechanical properties in the dry and wet states. Moreover, it was demonstrated that plasma treated P-cocoon membranes can be washed and dried, at least 3 times, without losing their physicochemical properties, allowing their reuse, which make them particularly interesting candidates for eco-friendly microfluidic substrates, taking into consideration circular economy and sustainability (*e.g.* preventing waste and one time use).

4. Conclusion

Bombyx mori cocoons and electrospun silk fibroin were used to manufacture substrates for a next generation of sustainable portable analytical devices. The substrates consist of pressed cocoons and both oriented and randomly oriented electrospun fibers prepared from purified silk fibroin extracted from the same type of cocoon. Oxygen plasma treatment was applied to these samples to make them superhydrophilic, and a thorough characterization of their physicochemical properties and overall behavior when interacting with aqueous solutions was carried out, showing mechanical stability, thermal resistance,and ability for

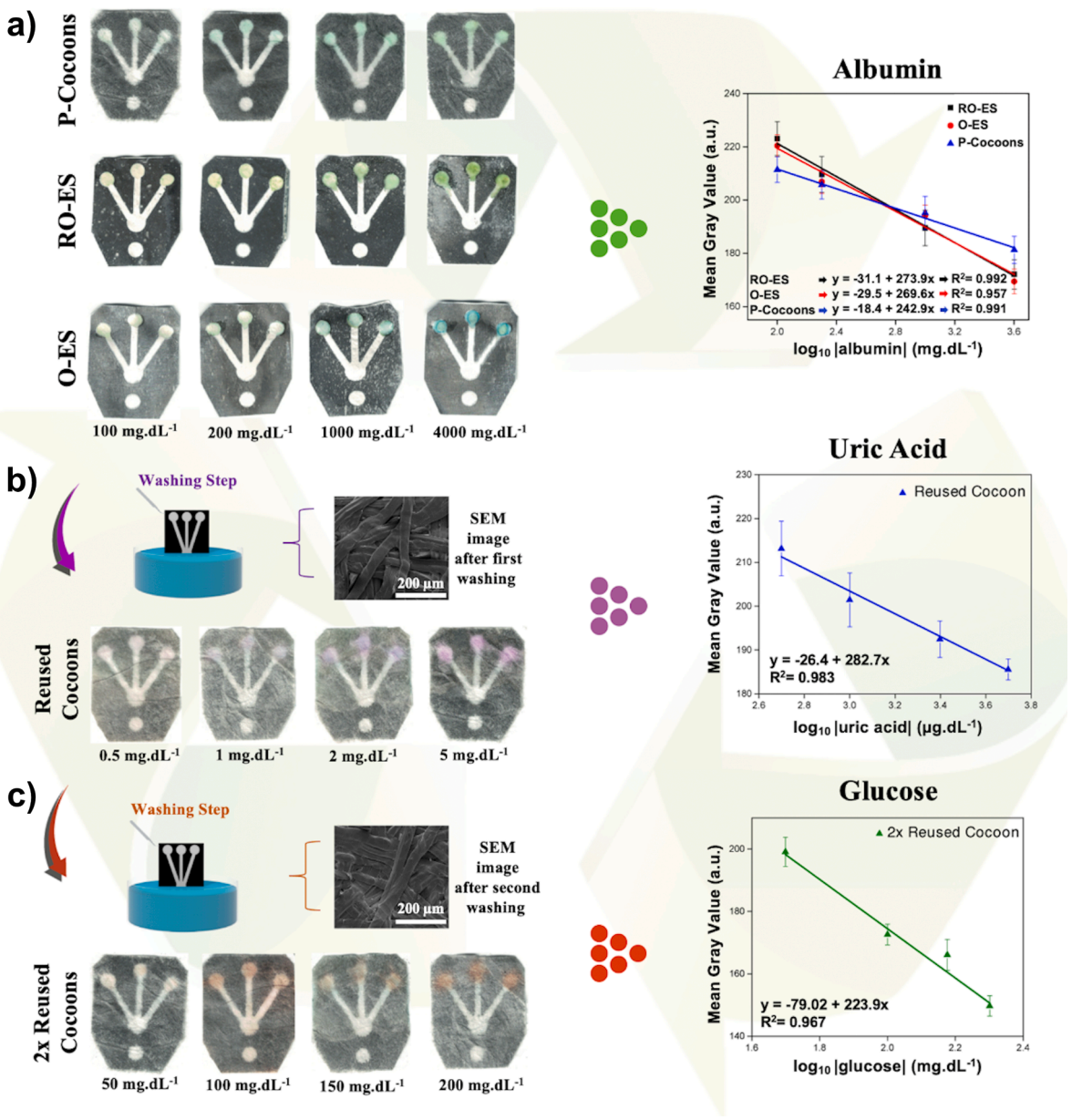

Fig. 5. Colorimetric albumin bioassay proofs of concept and corresponding calibration curves on wax-printed: **a)** P-cocoons, RO-ES and O-ES substrates w/ plasma treatment. **b)** Colorimetric uric acid assays in reused P-cocoons, corresponding calibration curves and SEM image of P-cocoons microstructure after the washing process. **c)** Colorimetric glucose assays on two times reused P-cocoons, corresponding calibration curves and SEM image of P-cocoons microstructure after the second washing process.

capillary flow. Plasma treated pressed *Bombyx mori* cocoons in particular show superhydrophilicity, capillary flow rates of 44.8 ± 3.75 mm. min^{-1}, and mechanical resistance, with Young's modulus values of 592.13 ± 19.83 MPa (dry conditions) and 377.2 ± 14.39 MPa (wet conditions). Proofs of concept were produced by wax-printing hydrophobic barriers according to a pattern composed of insertion and reaction chambers joined by channels. Although electrospun samples allow higher printing quality, an albumin colorimetric assay showed that all substrates performed well and a suitable quantity of fluid was contained inside the chambers, allowing formation of the colored complexes. As pressed *Bombyx mori* cocoons require no further processing besides pressing and plasma treatment, they were selected for subsequent cleaning and further colorimetric testing to evaluate their possible reuse. Uric acid and glucose tests were successfully carried out after in between cleaning procedures, showing that reutilization is possible without compromising substrate and printed microstructure and, therefore, system functionality.

Bombyx mori cocoons as well as silk fibroin electrospun mats are demonstrated to be suitable substrates for the development of portable analytical devices. Natural-based materials as reusable substrates are so proposed for a next generation of portable analytical systems with reduced environmental impact, not only for colorimetric assays, but also for other methods of detection in areas such as biomedicine, environmental monitoring, or food quality control, among others.

Author contribution statement

Ricardo Brito-Pereira: Conceptualization, Methodology, Investigation, Validation, Data Curation, Visualization, Writing - Original Draft. André S. Macedo: Investigation, Validation, Data Curation, Visualization, Writing - Original Draft. Clarisse Ribeiro: Resources, Methodology, Investigation, Validation, Data Curation. Vanessa F. Cardoso:

Table 2
Main properties of commercial paper-based membranes, the developed P-cocoons and the ES SF membranes as substrates for microfluidic applications.

	Whatman™ n°.1 [23]	*Millipore HF090* [23]	P-cocoons	ES SF membranes	
Natural origin	Yes	Yes	Yes	Yes	Yes
Chemical processes (including bleaching)	Yes	Yes	No	No	No
Morphology	Randomly oriented cellulose microfibres	Spherulitic-like nitrocellulose porous structure*	Randomly oriented microfibres	Oriented microfibres	Randomly oriented microfibres
Wettability	Superhydrophilic	Superhydrophilic	Superhydrophilic after plasma treatment		
Capillary flow ($mm.min^{-1}$)	44.1±1.13	25.0±3.4**	44.8 ± 3.75	82.1 ± 4.95	46.5 ± 2.05
Wax print quality	Poor (expands 1.2 mm after curing)	High	Good	High	High
Colorimetric detection quality	Good	Good (only in the back side)	Good	Good	Acceptable
Mechanical properties (dry/wet)	+/-	+/+*	++/++	+/+	+/+
Reusable	No	No	Yes (washable)		

* laminated membrane with backing material. Scrapes easily.
** tailorable according to Millipore type.

Conceptualization, Resources, Methodology, Data Curation, Supervision, Writing - review & editing, Funding acquisition. Senentxu Lanceros-Méndez: Conceptualization, Resources, Methodology, Supervision, Writing - review, Funding acquisition.

Declaration of Competing Interest

The authors declare that they have no known competing financial interests or personal relationships that could have appeared to influence the work reported in this paper.

Acknowledgments

This work was supported by the Portuguese Foundation for Science and Technology (FCT) under strategic funding UID/FIS/04650/2020, UIDB/04436/2020, UIDP/04436/2020 and project PTDC/EMD-EMD/28159/2017 (POCI-01–0145-FEDER-028159). The authors also thank FCT for financial support under grants SFRH/BD/140698/2018 (R.B.P.), 2020.09218.BD (A.S.M.), 2020.04163.CEECIND (C.R.) and 2020.02304.CEECIND (V.F.C.). Finally, the authors acknowledge funding by Spanish State Research Agency (AEI) and the European Regional Development Fund (ERFD) through the project PID2019–106099RB-C43/AEI/10.13039/501100011033 and from the Basque Government Industry Departments under the ELKARTEK program. Finally, the authors also thank Dr. J. Borges and Prof. F. Vaz for experimental support.

References

[1] T. Tönnies, S. Röckl, A. Hoyer, C. Heidemann, J. Baumert, Y. Du, C. Scheidt-Nave, R. Brinks, Projected number of people with diagnosed Type 2 diabetes in Germany in 2040, Diabet. Med. 36 (2019) 1217–1225, https://doi.org/10.1111/dme.13902.
[2] N. Van Der Schaft, A. Brahimaj, K.-.X. Wen, O.H. Franco, A. Dehghan, The association between serum uric acid and the incidence of prediabetes and type 2 diabetes mellitus: the Rotterdam Study, PLoS One 12 (2017), https://doi.org/10.1371/journal.pone.0179482.
[3] A. Virdis, S. Masi, E. Casiglia, V. Tikhonoff, A.F.G. Cicero, A. Ungar, G. Rivasi, M. Salvetti, C.M. Barbagallo, M. Bombelli, G. Grassi, C. Borghi, Identification of the Uric Acid Thresholds Predicting an Increased Total and Cardiovascular Mortality over 20 Years, Hypertension (2020) 302–308, https://doi.org/10.1161/HYPERTENSIONAHA.119.13643.
[4] E.P. De Oliveira, R.C. Burini, High plasma uric acid concentration: causes and consequences, Diabetol. Metab. Syndr. (2012) 4, https://doi.org/10.1186/1758-5996-4-12.
[5] A. Gatta, A. Verardo, M. Bolognesi, Hypoalbuminemia, Intern. Emerg. Med. 7 (2012) 193–199, https://doi.org/10.1007/s11739-012-0802-0.
[6] P.B. Soeters, R.R. Wolfe, A. Shenkin, Hypoalbuminemia: pathogenesis and clinical significance, J. Parenter. Enter. Nutr. 43 (2019) 181–193, https://doi.org/10.1002/jpen.1451.
[7] C. Zhao, L. Chen, G. Zhong, Q. Wu, J. Liu, X. Liu, A portable analytical system for rapid on-site determination of total nitrogen in water, Water Res. 202 (2021), https://doi.org/10.1016/j.watres.2021.117410.
[8] X. Weng, S. Neethirajan, Ensuring food safety: quality monitoring using microfluidics, Trends Food Sci. Technol. 65 (2017) 10–22, https://doi.org/10.1016/j.tifs.2017.04.015.
[9] A. Sanati, Y. Esmaeili, E. Bidram, L. Shariati, M. Rafienia, S. Mahshid, O. Parlak, Recent advancement in electrode materials and fabrication, microfluidic designs, and self-powered systems for wearable non-invasive electrochemical glucose monitoring, Appl. Mater. Today. (2022) 26, https://doi.org/10.1016/j.apmt.2021.101350.
[10] A.W. Martinez, S.T. Phillips, M.J. Butte, G.M. Whitesides, Patterned Paper as a Platform for Inexpensive, Low-Volume, Portable Bioassays, Angew. Chemie. 119 (2007) 1340–1342, https://doi.org/10.1002/ange.200603817.
[11] C. Li, M. Boban, S.A. Snyder, S.P.R. Kobaku, G. Kwon, G. Mehta, A. Tuteja, Paper-based surfaces with extreme wettabilities for novel, open-channel microfluidic devices, Adv. Funct. Mater. 26 (2016) 6121–6131, https://doi.org/10.1002/adfm.201601821.
[12] A.W. Lang, A.M. Österholm, J.R. Reynolds, Paper-based electrochromic devices enabled by nanocellulose-coated substrates, Adv. Funct. Mater. (2019) 29, https://doi.org/10.1002/adfm.201903487.
[13] R. Tang, M.Y. Xie, M. Li, L. Cao, S. Feng, Z. Li, F. Xu, Nitrocellulose Membrane for Paper-based Biosensor, Appl. Mater. Today. (2022) 26, https://doi.org/10.1016/j.apmt.2021.101305.
[14] D.A. Bruzewicz, M. Reches, G.M. Whitesides, Low-cost printing of poly (dimethylsiloxane) barriers to define microchannels in paper, Anal. Chem. 80 (2008) 3387–3392, https://doi.org/10.1021/ac702605a.
[15] X. Li, J. Tian, G. Garnier, W. Shen, Fabrication of paper-based microfluidic sensors by printing, Colloids Surf. B Biointerfaces 76 (2010) 564–570, https://doi.org/10.1016/j.colsurfb.2009.12.023.
[16] W. Dungchai, O. Chailapakul, C.S. Henry, A low-cost, simple, and rapid fabrication method for paper-based microfluidics using wax screen-printing, Analyst 136 (2011) 77–82, https://doi.org/10.1039/c0an00406e.
[17] P. Preechakasedkit, W. Siangproh, N. Khongchareonporn, N. Ngamrojanavanich, O. Chailapakul, Development of an automated wax-printed paper-based lateral flow device for alpha-fetoprotein enzyme-linked immunosorbent assay, Biosens. Bioelectron. 102 (2018) 27–32, https://doi.org/10.1016/j.bios.2017.10.051.
[18] C. Dixon, J. Lamanna, A.R. Wheeler, Printed Microfluidics, Adv. Funct. Mater. (2017) 27, https://doi.org/10.1002/adfm.201604824.
[19] M. Benhabib, X.J. Li, Low-cost Assays in Paper-Based Microfluidic Biomedical Devices, 2013, https://doi.org/10.1533/9780857097040.4.492.
[20] S.K. Vashist, P.B. Luppa, L.Y. Yeo, A. Ozcan, J.H.T. Luong, Emerging Technologies for Next-Generation Point-of-Care Testing, Trends Biotechnol. 33 (2015) 692–705, https://doi.org/10.1016/j.tibtech.2015.09.001.
[21] X. Mao, T.-.E. Du, Y. Wang, L. Meng, Disposable dry-reagent cotton thread-based point-of-care diagnosis devices for protein and nucleic acid test, Biosens. Bioelectron. 65 (2015) 390–396, https://doi.org/10.1016/j.bios.2014.10.053.
[22] E.S. Pimentel, R. Brito-Pereira, T. Marques-Almeida, C. Ribeiro, F. Vaz, S. Lanceros-Mendez, V.F. Cardoso, Tailoring electrospun Poly(l -lactic acid) Nanofibers as Substrates for Microfluidic applications, ACS Appl. Mater. Interfaces. 12 (2020) 60–69, https://doi.org/10.1021/acsami.9b12461.
[23] R. Brito-Pereira, A.S. Macedo, C.R. Tubio, S. Lanceros-Méndez, V.F. Cardoso, Fluorinated polymer membranes as advanced substrates for portable analytical systems and their proof of concept for colorimetric bioassays, ACS Appl. Mater. Interfaces. 13 (2021) 18065–18076, https://doi.org/10.1021/acsami.1c00227.
[24] P. Bajpai, Green chemistry and sustainability in pulp and paper industry, 2015. https://doi.org/10.1007/978-3-319-18744-0.
[25] P.R. van Oel, A.Y. Hoekstra, Towards quantification of the water footprint of paper: a first estimate of its consumptive component, Water Resour. Manag. 26 (2012) 733–749, https://doi.org/10.1007/s11269-011-9942-7.
[26] E.A. Olivetti, J.M. Cullen, Toward a sustainable materials system, Science (80-.) 360 (2018) 1396–1398, https://doi.org/10.1126/science.aat6821.
[27] M. Minoglou, S. Gerassimidou, D. Komilis, Healthcare waste generation worldwide and its dependence on socio-economic and environmental factors, Sustain (2017) 9, https://doi.org/10.3390/su9020220.
[28] B. Kaiser, P.D. Eagan, H. Shaner, Solutions to health care waste: life-cycle thinking and "green" purchasing, Environ. Health Perspect. 109 (2001) 205–207, https://doi.org/10.1289/ehp.01109205.

[29] W.R. Stahel, The circular economy, Nature 531 (2016) 435–438, https://doi.org/10.1038/531435a.
[30] J.-.W. Seo, H. Kim, K. Kim, S.Q. Choi, H.J. Lee, Calcium-modified silk as a biocompatible and strong adhesive for epidermal electronics, Adv. Funct. Mater. (2018) 28, https://doi.org/10.1002/adfm.201800802.
[31] I.C. Um, H. Kweon, Y.H. Park, S. Hudson, Structural characteristics and properties of the regenerated silk fibroin prepared from formic acid, Int. J. Biol. Macromol. 29 (2001) 91–97, https://doi.org/10.1016/S0141-8130(01)00159-3.
[32] Z. Liu, Z. Zhou, S. Zhang, L. Sun, Z. Shi, Y. Mao, K. Liu, T.H. Tao, Print-to-pattern": silk-based water lithography, Small 14 (2018), https://doi.org/10.1002/smll.201802953.
[33] A. Motta, L. Fambri, C. Migliaresi, Regenerated silk fibroin films: thermal and dynamic mechanical analysis, Macromol. Chem. Phys. 203 (2002) 1658–1665, https://doi.org/10.1002/1521-3935(200207)203:10/11<1658::AID−MACP1658>3.0.CO;2-3.
[34] L.W. Tien, F. Wu, M.D. Tang-Schomer, E. Yoon, F.G. Omenetto, D.L. Kaplan, Silk as a multifunctional biomaterial substrate for reduced glial scarring around brain-penetrating electrodes, Adv. Funct. Mater. 23 (2013) 3185–3193, https://doi.org/10.1002/adfm.201203716.
[35] D.N. Rockwood, R.C. Preda, T. Yücel, X. Wang, M.L. Lovett, D.L. Kaplan, Materials fabrication from Bombyx mori silk fibroin, Nat. Protoc. 6 (2011) 1612–1631, https://doi.org/10.1038/nprot.2011.379.
[36] B. Kundu, R. Rajkhowa, S.C. Kundu, X. Wang, Silk fibroin biomaterials for tissue regenerations, Adv. Drug Deliv. Rev. 65 (2013) 457–470, https://doi.org/10.1016/j.addr.2012.09.043.
[37] X. Gao, J. Gou, L. Zhang, S. Duan, C. Li, A silk fibroin based green nano-filter for air filtration, RSC Adv. 8 (2018) 8181–8189, https://doi.org/10.1039/c7ra12879g.
[38] Y.-.F. Liu, M.-.H. An, Y.-.G. Bi, D. Yin, J. Feng, H.-.B. Sun, Flexible 34strate, IEEE Photonics J 9 (2017), https://doi.org/10.1109/JPHOT.2017.2740618.
[39] D.-.H. Kim, J. Viventi, J.J. Amsden, J. Xiao, L. Vigeland, Y.-.S. Kim, J.A. Blanco, B. Panilaitis, E.S. Frechette, D. Contreras, B. Litt, J.A. Rogers, Dissolvable films of silk fibroin for ultrathin conformal bio-integrated electronics, Nat. Mater. 9 (2010) 511–517, https://doi.org/10.1038/nmat2745.
[40] Y. Liu, L.-.Q. Tao, D.-.Y. Wang, T.-.Y. Zhang, Y. Yang, T.-.L. Ren, Flexible, highly sensitive pressure sensor with a wide range based on graphene-silk network structure, Appl. Phys. Lett. (2017) 110, https://doi.org/10.1063/1.4978374.
[41] X. You, J.J. Pak, Graphene-based field effect transistor enzymatic glucose biosensor using silk protein for enzyme immobilization and device substrate, Sensors Actuators, B Chem 202 (2014) 1357–1365, https://doi.org/10.1016/j.snb.2014.04.079.
[42] M.S. Mannoor, H. Tao, J.D. Clayton, A. Sengupta, D.L. Kaplan, R.R. Naik, N. Verma, F.G. Omenetto, M.C. McAlpine, Graphene-based wireless bacteria detection on tooth enamel, Nat. Commun. (2012) 3, https://doi.org/10.1038/ncomms1767.
[43] M. Xu, V.K. Yadavalli, Flexible biosensors for the impedimetric detection of protein targets using silk-conductive polymer biocomposites, ACS Sensors 4 (2019) 1040–1047, https://doi.org/10.1021/acssensors.9b00230.
[44] T. Choudhary, G.P. Rajamanickam, D. Dendukuri, Woven electrochemical fabric-based test sensors (WEFTS): a new class of multiplexed electrochemical sensors, Lab Chip 15 (2015) 2064–2072, https://doi.org/10.1039/c5lc00041f.
[45] G.H. Altman, F. Diaz, C. Jakuba, T. Calabro, R.L. Horan, J. Chen, H. Lu, J. Richmond, D.L. Kaplan, Silk-based biomaterials, Biomaterials 24 (2003) 401–416, https://doi.org/10.1016/S0142-9612(02)00353-8.
[46] N.P.C. Horrocks, F. Vollrath, C. Dicko, The silkmoth cocoon as humidity trap and waterproof barrier, Comp. Biochem. Physiol. - A Mol. Integr. Physiol. 164 (2013) 645–652, https://doi.org/10.1016/j.cbpa.2013.01.023.
[47] B. Tulachan, S.K. Meena, R.K. Rai, C. Mallick, T.S. Kusurkar, A.K. Teotia, N. K. Sethy, K. Bhargava, S. Bhattacharya, A. Kumar, S.K. Singh, M. Das, Electricity from the silk cocoon membrane, Sci. Rep. (2014) 4, https://doi.org/10.1038/srep05434.
[48] H. Wang, S. Duan, M. Wang, S. Wei, Y. Chen, W. Chen, Y. Li, S. Ding, Silk cocoon membrane-based immunosensing assay for red blood cell antigen typing, Sensors Actuators, B Chem (2020) 320, https://doi.org/10.1016/j.snb.2020.128376.
[49] J. Doshi, D.H. Reneker, Electrospinning process and applications of electrospun fibers, J. Electrostat. 35 (1995) 151–160, https://doi.org/10.1016/0304-3886(95)00041-8.
[50] M. Farokhi, F. Mottaghitalab, R.L. Reis, S. Ramakrishna, S.C. Kundu, Functionalized silk fibroin nanofibers as drug carriers: advantages and challenges, J. Control. Rel. 321 (2020) 324–347, https://doi.org/10.1016/j.jconrel.2020.02.022.
[51] S.-.D. Wang, Q. Ma, K. Wang, H.-.W. Chen, Improving antibacterial activity and biocompatibility of bioinspired electrospinning silk fibroin nanofibers modified by graphene oxide, ACS Omega 3 (2017) 406–413, https://doi.org/10.1021/acsomega.7b01210.
[52] G. Zhao, X. Zhang, B. Li, G. Huang, F. Xu, X. Zhang, Solvent-free fabrication of carbon nanotube/silk fibroin electrospun matrices for enhancing cardiomyocyte functionalities, ACS Biomater. Sci. Eng. 6 (2020) 1630–1640, https://doi.org/10.1021/acsbiomaterials.9b01682.
[53] J. Lai, B. Sunderland, J. Xue, S. Yan, W. Zhao, M. Folkard, B.D. Michael, Y. Wang, Study on hydrophilicity of polymer surfaces improved by plasma treatment, Appl. Surf. Sci. 252 (2006) 3375–3379, https://doi.org/10.1016/j.apsusc.2005.05.038.
[54] L. Jeong, I.-.S. Yeo, H.N. Kim, Y.I. Yoon, D.H. Jang, S.Y. Jung, B.-.M. Min, W. H. Park, Plasma-treated silk fibroin nanofibers for skin regeneration, Int. J. Biol. Macromol. 44 (2009) 222–228, https://doi.org/10.1016/j.ijbiomac.2008.12.008.
[55] D.M. Correia, C. Ribeiro, G. Botelho, J. Borges, C. Lopes, F. Vaz, S.A.C. Carabineiro, A.V. MacHado, S. Lanceros-Méndez, Superhydrophilic poly(l-lactic acid) electrospun membranes for biomedical applications obtained by argon and oxygen plasma treatment, Appl. Surf. Sci. 371 (2016) 74–82, https://doi.org/10.1016/j.apsusc.2016.02.121.
[56] R. Brito-Pereira, D.M. Correia, C. Ribeiro, A. Francesko, I. Etxebarria, L. Pérez-Álvarez, J.L. Vilas, P. Martins, S. Lanceros-Mendez, Silk fibroin-magnetic hybrid composite electrospun fibers for tissue engineering applications, Compos. Part B Eng. 141 (2018) 70–75, https://doi.org/10.1016/j.compositesb.2017.12.046.
[57] D.M. Correia, C. Ribeiro, V. Sencadas, G. Botelho, S.A.C. Carabineiro, J.L. G. Ribelles, S. Lanceros-Méndez, Influence of oxygen plasma treatment parameters on poly(vinylidene fluoride) electrospun fiber mats wettability, Prog. Org. Coatings. 85 (2015) 151–158, https://doi.org/10.1016/j.porgcoat.2015.03.019.
[58] Y. Ishii, H. Sakai, H. Murata, A new electrospinning method to control the number and a diameter of uniaxially aligned polymer fibers, Mater. Lett. 62 (2008) 3370–3372, https://doi.org/10.1016/j.matlet.2008.03.038.
[59] I. Unalan, O. Colpankan, A.Z. Albayrak, C. Gorgun, A.S. Urkmez, Biocompatibility of plasma-treated poly(3-hydroxybutyrate-co-3-hydroxyvalerate) nanofiber mats modified by silk fibroin for bone tissue regeneration, Mater. Sci. Eng. C. 68 (2016) 842–850, https://doi.org/10.1016/j.msec.2016.07.054.
[60] R.F.P. Pereira, R. Gonçalves, H.M.R. Gonçalves, D.M. Correia, C.M. Costa, M. M. Silva, S. Lanceros-Méndez, V. de Zea Bermudez, Plasma-treated Bombyx mori cocoon separators for high-performance and sustainable lithium-ion batteries, Mater. Today Sustain. 9 (2020), https://doi.org/10.1016/j.mtsust.2020.100041.
[61] M.M. Maciel, S. Ribeiro, C. Ribeiro, A. Francesko, A. Maceiras, J.L. Vilas, S. Lanceros-Méndez, Relation between fiber orientation and mechanical properties of nano-engineered poly(vinylidene fluoride) electrospun composite fiber mats, Compos. Part B Eng. 139 (2018) 146–154, https://doi.org/10.1016/j.compositesb.2017.11.065.
[62] C.S. Ki, J.W. Kim, H.J. Oh, K.H. Lee, Y.H. Park, The effect of residual silk sericin on the structure and mechanical property of regenerated silk filament, Int. J. Biol. Macromol. 41 (2007) 346–353, https://doi.org/10.1016/j.ijbiomac.2007.05.005.
[63] D. Gupta, A. Agrawal, A. Rangi, Extraction and characterization of silk sericin, Indian J. Fibre Text. Res. 39 (2014) 364–372.
[64] A. Reizabal, R. Brito-Pereira, M.M. Fernandes, N. Castro, V. Correia, C. Ribeiro, C. M. Costa, L. Perez, J.L. Vilas, S. Lanceros-Méndez, Silk fibroin magnetoactive nanocomposite films and membranes for dynamic bone tissue engineering strategies, Materialia 12 (2020), https://doi.org/10.1016/j.mtla.2020.100709.
[65] O. Deveoglu, R. Karadag, A. Spinella, E.T. Guzel, Examination of dyeing properties on silk of some flavonoids by spectroscopic techniques, J. Nat. Fibers. 18 (2021) 238–249, https://doi.org/10.1080/15440478.2019.1616650.
[66] E. Iizuka, Size dependency of the physical properties of Bombyx silk, J. Sericultural Sci. Japan. 65 (1996) 102–108.
[67] S. Mazzi, E. Zulker, J. Buchicchio, B. Anderson, X. Hu, Comparative thermal analysis of Eri, Mori, Muga, and Tussar silk cocoons and fibroin fibers, J. Therm. Anal. Calorim. 116 (2014) 1337–1343, https://doi.org/10.1007/s10973-013-3631-0.
[68] P. Cebe, B.P. Partlow, D.L. Kaplan, A. Wurm, E. Zhuravlev, C. Schick, Silk I and Silk II studied by fast scanning calorimetry, Acta Biomater 55 (2017) 323–332, https://doi.org/10.1016/j.actbio.2017.04.001.
[69] N. Agarwal, D.A. Hoagland, R.J. Farris, Effect of moisture absorption on the thermal properties of Bombyx mori silk fibroin films, J. Appl. Polym. Sci. 63 (1997) 401–410, https://doi.org/10.1002/(SICI)1097-4628(19970118)63:3<401::AID−APP17>3.0.CO;2-2.
[70] D. Tian, Y. Song, L. Jiang, Patterning of controllable surface wettability for printing techniques, Chem. Soc. Rev. 42 (2013) 5184–5209, https://doi.org/10.1039/c3cs35501b.
[71] P.K. Szewczyk, D.P. Ura, S. Metwally, J. Knapczyk-Korczak, M. Gajek, M. M. Marzec, A. Bernasik, U. Stachewicz, Roughness and fiber fraction dominated wetting of electrospun fiber-based porous meshes, Polymers (Basel) 11 (2019), https://doi.org/10.3390/polym11010034.